Rigorous Susceptibility-Based Design of Generalized Huygens' Metasurface Radomes

Amit Shaham and Ariel Epstein
Andrew and Erna Viterbi Faculty of Electrical and Computer Engineering, Technion – Israel Institute of Technology, Haifa, 3200003, Israel. samitsh@campus.technion.ac.il, epsteina@ee.technion.ac.il

***Abstract*—In this paper, we utilize the profound generalized Huygens' condition (GHC) to rigorously devise all-angle transparent metasurface (MS) radomes. We extend our recent configuration of double-layered admittance-sheet cascades, which allows only one Huygens' condition to hold (at grazing angle), by incorporating a third middle layer; we thus fully satisfy Huygens' condition both at normal and grazing angles in closed form. Our meticulous analysis introduces a universal nonlocal link between macroscopic MS constituents and their corresponding effective meta-atom susceptibilities. Particularly, it reveals that the trilayered composite inevitably manifests effective normal susceptibilities overlooked by common tangentially-polarized MS design practices. A printed-circuit-board version of the radome is realized and inspected in theory and simulation. Its excellent observed performance validates the GHC in a fundamental practical situation and sets the stage to cutting-edge performance in advanced nonlocal wave-moulding functionalities.**

***Index Terms*—metasurfaces, radomes, antennas, generalized Huygens' condition, nonlocality, anti-reflective coatings.**

I. Introduction

Antenna radomes play several important roles in practical transceiver systems, e.g., airborne radars and communications. They traditionally provide mechanical protection against harsh outdoor conditions and visual concealment of the aerial and other related equipment [1]–[3]. Nowadays, owing to the rapid evolution of frequency selective surfaces (FSS), metamaterials, and metasurfaces (MS), they allow integration of numerous enhancements, such as frequency [4], angular [5], [6], and excessive power [7] filtering; beam and radiation-pattern shaping [8], [9]; and wide angle impedance matching (WAIM) [10].

Engineering-wise, it would often be preferable to utilize planar radomes due to their low profile and relatively easy fabrication. Could such devices be rendered electromagnetically transparent *for all angles* as well, they would completely relieve several commonly encountered constraints, e.g., electromagnetic coupling between antenna and radome and degradation of radiation pattern. They would thus enable more convenient and independent design procedure for the antenna.

So far, metamaterial effective-medium approaches have indeed aspired to achieve such a functionality [2], [11], [12]. They typically propose an arbitrary initial configuration, such as multilayered thin metallic patterns supported by dielectric substrates, and empirically optimize the inclusion geometries in simulations, based on volumetric bulk effective parameters, for instance, permittivity and permeability. Indeed, such optimizations can achieve excellent performance in certain scenarios, yet they are often short of fundamental insights and physical intuition. For example, essential queries may rise regarding the applicable range of substrate properties (thickness, permittivity, etc.) that ensure valid solutions; the optimality of the device and minimal number of degrees of freedom (e.g., number of layers) and simplest types of response to guarantee it; the underlying physical phenomena; and the existence of simple elementary design principles.

Very recently, we have revealed a profound framework, namely, the generalized Huygens' condition (GHC) [13], to address such issues. It universally states that planar all-angle transparency can be simply achieved by enforcing nothing more than vanishing reflection at *normal* and *grazing* incidence scenarios, provided deep-subwavelength thickness of the device. At the microscopic level, we have shown that the former is equivalent to the well-known standard Huygens' condition of balanced *tangential* electric and magnetic responses [14]–[19]; the latter unconventional Huygens' condition at grazing incidence, however, manifests another distinct balance between electric and *normal* magnetic components and establishes the dominant fulcrum of omnidirectional transparency.

Demonstrating the nonlocal foundations behind the GHC, we have further found a simple closed-form manner to enforce the crucial grazing-angle Huygens' condition by symmetrically coating thin dielectric slabs with two electrically polarizable admittance sheets compatible with standard printed-circuit-board (PCB) technology [13]. Fascinatingly, despite exhausting all its available degrees of freedom to fulfill this condition and, hence, inevitably deviating from the normal-incidence Huygens' condition, this double-layered structure still exhibits practical all-angle low reflectance, near-unity transmittance, and wavefront preservation, as desired.

In this paper, we extend this concept to achieve simultaneous stipulation of both normal- and grazing-incidence Huygens' conditions in such realistic designs, to thus perfectly meet the GHC in practice. To this end, we embed a third middle admittance layer into the previous double-layered PCB configuration. By applying standard generalized-sheet-transition-condition (GSTC) and transmission-line (TL) analyses, we rigorously formulate fundamental closed-form expressions for the effective susceptibility values attributed to the trilayered PCB cascade in terms of its constituent properties. We thus establish a universal and useful link between the macroscopically nonlocal MS-level design to its corresponding microscopic meta-atom level. Importantly, we unravel the

978-88-31299-09-1/24/$31.00 ©2024 IEEE

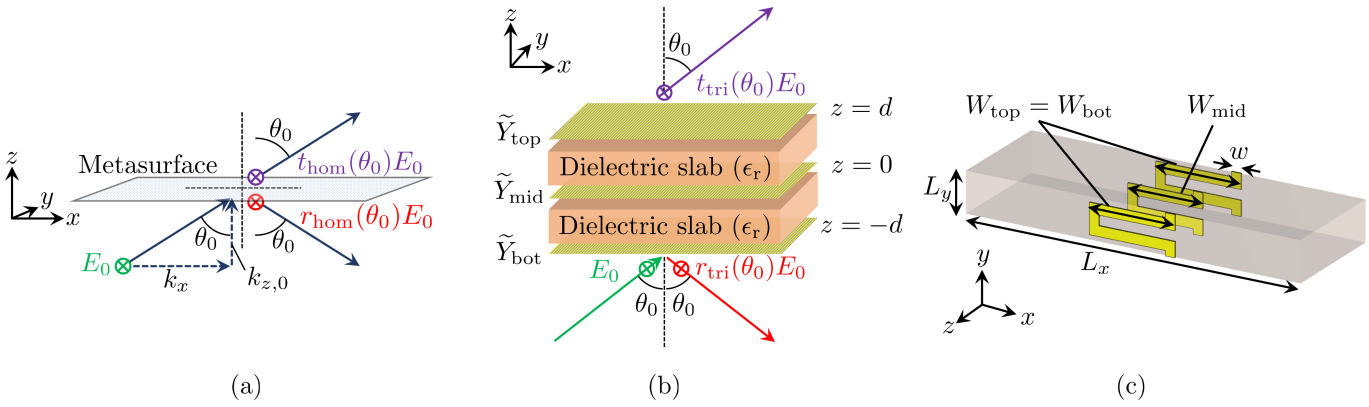

Fig. 1. Physical MS scattering configuration for (a) the thin homogenized sheet in Sec. II-A and (b) the symmetric ($\widetilde{Y}_{\rm top}=\widetilde{Y}_{\rm bot}$) trilayered cascade of admittance sheets separated by thin dielecrtic slabs. (c) PCB-compatible meander-line realization of the three admittance sheets at 20 GHz for Rogers RO3003 substrates of $\epsilon_{\rm r}=3$ and $d=30$ mil: $w=5$ mil trace width; $L_x=4.5$ mm $\approx 0.3\lambda_0$ periodicity along x; $L_y=4w=20$ mil $\approx 0.034\lambda_0$ periodicity along y; $W_{\rm top}=W_{\rm bot}=1.15$ mm and $W_{\rm mid}=1$ mm top, bottom, and middle meander widths after being fine-tuned to achieve the GHC (Sec. III).

role of each layer in determining the effective susceptibility values and, particularly, shed light on the nonintuitive normal component, which, albeit inevitably present, has so far eluded mainstream MS design considerations. Leveraging this powerful framework, we enforce the GHC and arrive at a closed-form solution demonstrated in simulations. Our observations of excellent performance validate the GHC as an invaluable tool and promise state-of-the-art future not only for transparent radomes, but also for other transmissive nonlocal applications in microwaves and optics.

II. Theory

A. Scattering off homogenized thin sheets (meta-atom level)

To establish solid grounds for our discussions throughout, we consider a 2D y-polarized transverse-electric (TE) configuration ($E_x=E_z=H_y=0$ and $\partial_y\equiv 0$) of a uniform MS situated at $z=0$ in free-space surroundings [Fig. 1(a)]. A TE plane wave described via $E_y^{\rm inc}(\vec{r})=E_0e^{-j(k_xx+k_{z,0}z)}$ impinges the MS from below ($z<0$) and results in specularly reflected ($E_y^{\rm ref}(\vec{r})$) and directly transmitted ($E_y^{\rm tran}(\vec{r})$) waves,

$$\begin{aligned} E_y^{\rm ref}(\vec{r}) &= r_{\rm hom}(\theta_0)\,E_0e^{-j(k_xx-k_{z,0}z)} \quad (z<0),\\ E_y^{\rm tran}(\vec{r}) &= t_{\rm hom}(\theta_0)\,E_0e^{-j(k_xx+k_{z,0}z)} \quad (z>0). \end{aligned} \tag{1}$$

E_0 is the amplitude of the incident wave, $k_x=k_0\sin\theta_0$ and $k_{z,0}=k_0\cos\theta_0$ are the tangential and normal wavenumbers in freespace, $k_0=\omega/c$ is the free-space wave number, θ_0 is the angle of incidence, $r_{\rm hom}(\theta_0)$ and $t_{\rm hom}(\theta_0)$ are the reflection and transmission coefficients of the homogenized sheet defined with respect to the $z=0$ reference plane, c is the speed of light, and harmonic time dependence of $e^{j\omega t}$ is assumed.

We focus on a particular TE MS configuration that involves only tangential electric ($\chi_{\rm ee}^{yy}$), tangential magnetic ($\chi_{\rm mm}^{xx}$), and normal magnetic ($\chi_{\rm mm}^{zz}$) surface susceptibilities. By following standard GSTC analysis [20]–[23], we have recently found that the scattering coefficients of the structure can be expressed via rational functions of the normal wave number $k_{z,0}$ [6], [13],

$$\begin{aligned} r_{\rm hom}(\theta_0) &= \frac{r_0+r_2\widetilde{k}_{z,0}^2}{d_0+d_1\widetilde{k}_{z,0}+d_2\widetilde{k}_{z,0}^2+d_3\widetilde{k}_{z,0}^3},\\ t_{\rm hom}(\theta_0) &= \frac{t_1\widetilde{k}_{z,0}+t_3\widetilde{k}_{z,0}^3}{d_0+d_1\widetilde{k}_{z,0}+d_2\widetilde{k}_{z,0}^2+d_3\widetilde{k}_{z,0}^3}, \end{aligned} \tag{2}$$

where

$$\begin{aligned} r_0&=-2\left(\widetilde{\chi}_{\rm ee}^{yy}+\widetilde{\chi}_{\rm mm}^{zz}\right), \quad r_2=2\left(\widetilde{\chi}_{\rm mm}^{xx}+\widetilde{\chi}_{\rm mm}^{zz}\right),\\ t_1&=-j\left[\left(\widetilde{\chi}_{\rm ee}^{yy}+\widetilde{\chi}_{\rm mm}^{zz}\right)\widetilde{\chi}_{\rm mm}^{xx}+4\right],\\ t_3&=j\widetilde{\chi}_{\rm mm}^{xx}\widetilde{\chi}_{\rm mm}^{zz}, \quad d_0=2\left(\widetilde{\chi}_{\rm ee}^{yy}+\widetilde{\chi}_{\rm mm}^{zz}\right),\\ d_1&=j\left[\left(\widetilde{\chi}_{\rm ee}^{yy}+\widetilde{\chi}_{\rm mm}^{zz}\right)\widetilde{\chi}_{\rm mm}^{xx}-4\right],\\ d_2&=2\left(\widetilde{\chi}_{\rm mm}^{xx}-\widetilde{\chi}_{\rm mm}^{zz}\right), \quad d_3=-j\widetilde{\chi}_{\rm mm}^{xx}\widetilde{\chi}_{\rm mm}^{zz} \end{aligned} \tag{3}$$

are the coefficients, and $\widetilde{\cdot}$ notation represents normalized dimensionless quantities with respect to wavenumber, i.e., $\widetilde{k}_{z,0}=k_{z,0}/k_0=\cos\theta_0$ and $\widetilde{\chi}=k_0\chi$. This form is highly useful since it can be conveniently interpreted as an analogy to standard frequency filters [24]–[26]: by tuning the susceptibility values, one may control the functionality of the angular filter and its properties. Besides providing a convenient tool to derive the GHC, as in [13], it shall serve a crucial role herein in deducing the aforementioned equivalence between the meta-atom and MS levels.

B. Scattering off trilayered admittance sheets (MS level)

To realize a practical all-angle transparent MS that meets the GHC we propose a configuration of three cascaded admittance sheets separated by thin dielectric substrates, as depicted in Fig. 1(b). The surface admittance values of the bottom ($z=-d$), middle ($z=0$), and top ($z=d$) layers are $\widetilde{Y}_{\rm bot}$, $\widetilde{Y}_{\rm mid}$, and $\widetilde{Y}_{\rm top}$, respectively, where $\widetilde{\cdot}$ represents normalization to the admittance of free space, $\widetilde{Y}=\eta_0Y$, the relative permittivity of the substrates is $\epsilon_{\rm r}$, and the overall thickness is $2d$. To avoid undesired effective bianisotropic response [27], we focus on symmetric configurations with $\widetilde{Y}_{\rm bot}=\widetilde{Y}_{\rm top}$.

As before, the composite is illuminated from below ($z < -d$) by a plane wave of $E_y^{\rm inc}(\vec{r}) = E_0 e^{-j[k_x x + k_{z,0}(z+d)]}$ impinging with angle θ_0, which is scattered into specularly reflected ($E_y^{\rm ref}(\vec{r})$) and directly transmitted ($E_y^{\rm tran}(\vec{r})$) waves,

$$\begin{aligned} E_y^{\rm ref}(\vec{r}) &= r_{\rm tri}(\theta_0)\, E_0 e^{-j[k_x x - k_{z,0}(z+d)]} \quad (z < -d), \\ E_y^{\rm tran}(\vec{r}) &= t_{\rm tri}(\theta_0)\, E_0 e^{-j[k_x x + k_{z,0}(z-d)]} \quad (z > d), \end{aligned} \tag{4}$$

where $r_{\rm tri}(\theta_0)$ and $t_{\rm tri}(\theta_0)$ are the reflection and transmission coefficients for the trilayered cascade defined with respect to the $z = \pm d$ reference planes.

Similarly to [13], [19], [27]–[29], we may represent the structure via an equivalent TL model and employ Snell's law and standard TL theory [26] to find the scattering coefficients. The tedious exact expressions (not shown) involve transcendental terms of the form

$$g_{\pm}\left(\widetilde{k}_{z,0}\right) = \left(\chi_{\rm r} + \widetilde{k}_{z,0}^2\right)^{\pm 1/2} \tan\left[k_0 d \left(\chi_{\rm r} + \widetilde{k}_{z,0}^2\right)^{1/2}\right], \tag{5}$$

where $\chi_{\rm r} = \epsilon_{\rm r} - 1$ is the susceptibility of the substrates.

Inspired by the simple rational form (2) obtained for the homogenized sheets in Sec. II-A and by the dominance of the grazing-incidence Huygens' condition [13], we derive the Taylor approximations of $g_{\pm}\left(\widetilde{k}_{z,0}\right)$ around the *grazing* angle of $\theta_0 = 90°$, for which $\widetilde{k}_{z,0} = 0$, i.e.,

$$g_{+}\left(\widetilde{k}_{z,0}\right) \approx p + u\widetilde{k}_{z,0}^2, \quad g_{-}\left(\widetilde{k}_{z,0}\right) \approx q, \tag{6}$$

where

$$\begin{aligned} p &= \chi_{\rm r}^{1/2} \tan\left(\chi_{\rm r}^{1/2} k_0 d\right) = \mathcal{O}\left(\chi_{\rm r} k_0 d\right), \\ q &= \chi_{\rm r}^{-1/2} \tan\left(\chi_{\rm r}^{1/2} k_0 d\right) = \mathcal{O}\left(k_0 d\right), \\ u &= \frac{1}{2}\left[q + k_0 d \sec^2\left(\chi_{\rm r}^{1/2} k_0 d\right)\right] = \mathcal{O}\left(k_0 d\right) \end{aligned} \tag{7}$$

are the coefficients, which depend solely on the substrate properties and frequency, namely, $k_0 d$ and $\chi_{\rm r}$. These approximations apply to all the angles of incidence ($-90° < \theta_0 < 90°$) when the substrates are electromagnetically thin compared to a wavelength in free space, i.e., $\frac{1}{3}(k_0 d)^2 \ll 1$, similarly in spirit to the general assumptions behind the GSTCs [20]–[23].

Remarkably, when we substitute (6) in the scattering coefficients of (4), we obtain the same rational form of (2), i.e.,

$$\begin{aligned} r_{\rm tri}(\theta_0) &= \frac{\rho_0 + \rho_2 \widetilde{k}_{z,0}^2}{\delta_0 + \delta_1 \widetilde{k}_{z,0} + \delta_2 \widetilde{k}_{z,0}^2 + \delta_3 \widetilde{k}_{z,0}^3}, \\ t_{\rm tri}(\theta_0) &= \frac{\tau_1 \widetilde{k}_{z,0} + \tau_3 \widetilde{k}_{z,0}^3}{\delta_0 + \delta_1 \widetilde{k}_{z,0} + \delta_2 \widetilde{k}_{z,0}^2 + \delta_3 \widetilde{k}_{z,0}^3}, \end{aligned} \tag{8}$$

where the coefficients ρ_0, ρ_2, δ_0, δ_1, δ_2, δ_3 can be expressed in terms of the substrate-related properties, p , q, and u, and the admittance values, $\widetilde{Y}_{\rm top}(= \widetilde{Y}_{\rm bot})$ and $\widetilde{Y}_{\rm mid}$ (the explicit cumbersome expressions are not shown here for brevity). This striking similarity between the rational forms of (2) and (8) heavily implies a fundamental link between the meta-atom level structure in Sec. II-A and the MS analyzed in this section, which we reveal in the following subsection.

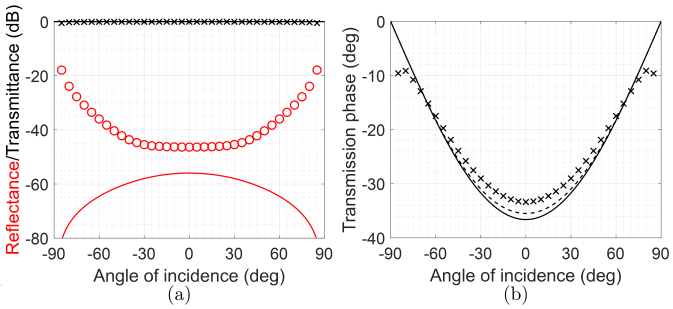

Fig. 2. (a) Reflectance (red) and transmittance (black) for the exact analytical TL-model (solid lines), equivalent susceptibility approximation (dashed lines, which coincide with the solid lines), and full-wave simulations of the realistic design ($\times$ and $\circ$ markers) (b) Transmission phase: exact TL model (solid line), equivalent susceptibility approximation [(2), (3), and (9), dashed lines], and full-wave simulations ($\times$ markers).

C. Equivalence relations between meta-atom and MS levels

In principle, as the GSTCs [20]–[23] are capable of universally describing the electromagnetic behavior of any thin sheet, we seek to fundamentally connect the macroscopic MS design in Sec. II-B to the microscopic meta-atom analysis in Sec. II-A in their light. We therefore enforce equality between the rational functions (2) and (8) by means of setting their coefficients proportional to each other with the same proportionality constant and following lengthy algebraic manipulations to obtain a consistent solution. Indeed, assuming that the substrates are also thin compared to a dielectric wavelength, namely, $\frac{1}{3}\chi_{\rm r}(k_0 d)^2 \ll 1$ (congruently with the GSTCs [20]–[23]), we find that (2) and (8) practically coincide for *all* angles of incidence *only* when the effective susceptibility values of

$$\begin{aligned} \widetilde{\chi}_{\rm ee}^{yy} &= \frac{4\left[1 + (p+u)\, q\right]}{q\left(2 + jq\widetilde{Y}_{\rm mid}\right)} - \frac{2\left(1 + jq\widetilde{Y}_{\rm top}\right)}{q}, \\ \widetilde{\chi}_{\rm mm}^{xx} &= \frac{2q}{1 + jq\widetilde{Y}_{\rm top}}, \quad \widetilde{\chi}_{\rm mm}^{zz} = -\frac{4u}{2 + jq\widetilde{Y}_{\rm mid}} \end{aligned} \tag{9}$$

are chosen.

Equation (9) has several far-reaching implications. First, it rigorously states that the space $-d < z < d$ occupied by the MS in Fig. 1(b) can be effectively replaced by a zero-thickness sheet of the susceptibilities described by the closed form of (9), as in Fig. 1(a). Second, it shows that normal susceptibilities are an indispensable integral part of the effective response, which has not been considered in previous approaches to engineering Huygens' MSs, e.g., [19], [27]–[29]: these schemes considered only the tangential responses ($\widetilde{\chi}_{\rm ee}^{yy}$ and $\widetilde{\chi}_{\rm mm}^{xx}$), which, in the absence of the normal response ($\widetilde{\chi}_{\rm mm}^{zz}$), yield accurate results only at normal incidence. Third, it emphasizes the dominant influence of the MS scattering behavior at grazing incidence on the entire angular range; its physical origins can be explained by macroscopic nonlocal mechanisms related to Maxwell's equations and multiple reflections [13], [30]. Lastly, it provides a powerful tool to emulate and control normal

susceptibilities by means of practical PCB-compatible sheets of mere tangential responses, as demonstrated in the following.

D. Generalized Huygens' condition

To achieve omnidirectional transparency, i.e., vanishing reflectance at all angles, one must set $\rho_0 = \rho_2 = 0$ [see (8)], or, by virtue of the equivalence derived in Sec. II-C, $r_0 = r_2 = 0$. Following (3), these requirements lead to the GHC [13],

$$\widetilde{\chi}_{\rm mm}^{xx} = \widetilde{\chi}_{\rm ee}^{yy} = -\widetilde{\chi}_{\rm mm}^{zz} \triangleq \widetilde{\chi}_{\rm GHC}, \tag{10}$$

where $\widetilde{\chi}_{\rm GHC}$ denotes the common value of the three susceptibilities, which, in general, serves as a degree of freedom to control the angular profile of the transmission phase.

Substituting (9) in (10) and solving a quadratic equation leads to two closed-form possible solutions for designing the sheet admittance values to achieve the perfect GHC (10) (both subconditions) for a given set of substrate properties p, q, u:

$$\begin{aligned} \widetilde{Y}_{\rm top} &= \widetilde{Y}_{\rm bot} = j\left(\frac{1}{q} \pm \sqrt{\frac{1+pq}{qu}}\right), \\ \widetilde{Y}_{\rm mid} &= j\left[\frac{2}{q} \pm \frac{2}{q}\sqrt{\frac{u\,(1+pq)}{q}}\right]. \end{aligned} \tag{11}$$

The first solution formed by taking the plus signs in (11) leads to extreme admittance values (order of $\mathcal{O}\left(\frac{1}{k_0 d}\right)$), which may impose practical realization difficulties. Therefore it is less preferable than the second minus-sign solution, which leads to moderate admittance values of $\widetilde{Y}_{\rm top} = \widetilde{Y}_{\rm bot} \approx -j\frac{1}{3}\chi_{\rm r} k_0 d$ and $\widetilde{Y}_{\rm mid} \approx -j\frac{4}{3}\chi_{\rm r} k_0 d$. Following (9), the latter solution results in the effective common susceptibility value of $\widetilde{\chi}_{\rm GHC} \approx 2k_0 d$. We have thus arrived at a rigorous and simple methodology to devise GHC-compatible trilayered admittance sheet cascades.

III. Results and discussion

To demonstrate and validate our theory, we design a generalized Huygens' MS PCB radome at 20 GHz according to the framework above. The substrates in our device are made of two commercial Rogers RO3003 slabs of relative permittivity $\epsilon_{\rm r} = 3$ and standard thickness $d = 30$ mil $\approx 0.051\lambda_0$ ($\lambda_0 \approx 15$ mm is the wavelength in free space at 20 GHz). These properties yield $\frac{1}{3}(k_0 d)^2 \approx 0.034 \ll 1$ and $\frac{1}{3}\chi_{\rm r}(k_0 d)^2 = 0.068 \ll 1$ and hence satisfy the subwavelength-thickness requirements above, for which our approximations hold.

Substituting these values in (7) and (11) yields $p \approx 0.686$, $q \approx 0.343$, $u \approx 0.369$, and the goal admittance values, $\widetilde{Y}_{\rm top} = \widetilde{Y}_{\rm bot} \approx -0.21$ and $\widetilde{Y}_{\rm mid} \approx -0.888$. According to (9), tuning the admittance of the layers to these values would lead to a generalized Huygens' MS of $\widetilde{\chi}_{\rm GHC} \approx 0.64$. We thereby set them and plot the angular dependence of the exact analytical TL-model predictions (solid lines) of reflectance [$|r_{\rm tri}(\theta_0)|^2$, red, Fig. 2(a)], transmittance [$|t_{\rm tri}(\theta_0)|^2$, black, Fig. 2(a)], and transmission phase [$\angle t_{\rm tri}(\theta_0)$, Fig. 2(b)]; for comparison, we also plot the predictions for the equivalent susceptibility approximation [(2), (3), and (9), dashed lines].

Excellent agreement is observed between the exact expression and the effective susceptibility model; remarkably small reflectance of $|r_{\rm tri}(\theta_0)|^2 < -55$ dB and large transmittance[1] $|t_{\rm tri}(\theta_0)|^2 \approx 1$ ensue for all angles ($-90^\circ < \theta_0 < 90^\circ$).

Next, we proceed to practically realize these favorable inductive admittance values at 20 GHz. To this end, we set a subwavelength unit-cell period of $L_x = 0.45$ mm $\approx 0.3\lambda_0$ along x and propose a generic set of printed copper meander lines [Fig. 1(c)] of $w = 5$ mil width (compatible with feature-size limitation of most PCB fabrication processes) and 18 μm thickness (standard 0.5 oz. deposition); the period along y is $L_y = 4w = 20$ mil $\approx 0.034\lambda_0$, as dictated from the trace geometry. By tuning the meander widths of the top and bottom layers (which share a common value, $W_{\rm top}$) and that of the middle one ($W_{\rm mid}$), we may, in principle, control the surface susceptance values $\mathrm{Im}\left[\widetilde{Y}_{\rm top}(W_{\rm top})\right]$ and $\mathrm{Im}\left[\widetilde{Y}_{\rm mid}(W_{\rm mid})\right]$.

To perform the tuning, we start by noting that $\widetilde{\chi}_{\rm mm}^{xx}$ depends only on the common admittance of the top and bottom layers $\widetilde{Y}_{\rm top}$. Therefore, we first discard the middle layer (keeping the top and bottom layers) and sweep the value of $W_{\rm top}$ (within the unit-cell boundaries) while monitoring the scattering coefficients at $\theta_0 = 0, 30^\circ$ in "CST Microwave Studio" (CST). These scattering coefficient results are then utilized to characterize the tangential magnetic susceptibility $\widetilde{\chi}_{\rm mm}^{xx}(W_{\rm top})$ associated with the structure, according to the method described in [31]. After establishing a look-up table (LUT) that links between meander dimensions and susceptibilities, we fix an appropriate width $W_{\rm top}$ to realize $\mathrm{Re}\left[\widetilde{\chi}_{\rm mm}^{xx}(W_{\rm top})\right] = \widetilde{\chi}_{\rm GHC} \approx 0.64$, as required above in (10).

Next, we introduce the middle meander and sweep $W_{\rm mid}$ (keeping the assigned value of $W_{\rm top}$ fixed), while characterizing and establishing LUTs for the electric $\widetilde{\chi}_{\rm ee}^{yy}(W_{\rm mid})$ and normal magnetic $\widetilde{\chi}_{\rm mm}^{zz}(W_{\rm mid})$ susceptibilities by following the same method executed for $\widetilde{\chi}_{\rm mm}^{xx}(W_{\rm top})$ above. We find the $W_{\rm mid}$ value for which $\mathrm{Re}\left[\widetilde{\chi}_{\rm ee}^{yy}(W_{\rm mid})\right]$ intersects with $-\mathrm{Re}\left[\widetilde{\chi}_{\rm mm}^{zz}(W_{\rm mid})\right]$ to thus fulfill the sensitive grazing-angle Huygens' condition to the utmost.

Ideally, the common value obtained for $\mathrm{Re}\left[\widetilde{\chi}_{\rm ee}^{yy}(W_{\rm mid})\right] = -\mathrm{Re}\left[\widetilde{\chi}_{\rm mm}^{zz}(W_{\rm mid})\right]$ should coincide with the value $\widetilde{\chi}_{\rm GHC} \approx 0.64$, as intended by our GHC design method (10). However, this value of intersection is found to deviate from the expected value (i.e., $\mathrm{Re}\left[\widetilde{\chi}_{\rm ee}^{yy}(W_{\rm mid})\right] = -\mathrm{Re}\left[\widetilde{\chi}_{\rm mm}^{zz}(W_{\rm mid})\right] \neq \widetilde{\chi}_{\rm GHC}$) due to near-field coupling between the outer layers and the middle one, such that Huygens' condition for normal incidence is not satisfied accurately. This can be fixed by fine-tuning the value of $W_{\rm top}$ and repeating the above procedure until all the three susceptibility values coincide precisely. In our scenario, this process yields the final optimal values of $W_{\rm top} = 1.15$ mm, $W_{\rm mid} = 1$ mm, which leads to a generalized Huygens' MS of $\mathrm{Re}\left(\widetilde{\chi}_{\rm ee}^{yy}\right) \approx \mathrm{Re}\left(\widetilde{\chi}_{\rm mm}^{xx}\right) \approx -\mathrm{Re}\left(\widetilde{\chi}_{\rm mm}^{zz}\right) \approx 0.6$, very close to the original theoretical prediction of $\widetilde{\chi}_{\rm GHC} \approx 0.64$.

We inspect the performance of the finalized design by plotting its full-wave reflectance [red $\circ$ markers in Fig. 2(a)],

[1] This performance is subject to our thinness assumptions above. A reference case-study when this approximation starts to break would be a thicker MS with $d = 80$ mil and $\epsilon_{\rm r} = 3$, i.e., $\frac{1}{3}(k_0 d)^2 \approx 0.24$ and $\frac{1}{3}\chi_{\rm r}(k_0 d)^2 \approx 0.48$, for which the minimal transmittance in $-90^\circ < \theta_0 < 90^\circ$ would deteriorate from $\sim 100\%$ to $\sim 93.7\%$ (~ -0.28 dB) when designed via (11).

transmittance [black $\times$ markers in Fig. 2(a)], and transmission phase [black $\times$ markers in Fig. 2(b)] vs. angle at 20 GHz. Excellent performance of omnidirectional transparency, which is limited only by inevitable copper and dielectric loss, is observed at the wide angular range of $-80^\circ \leq \theta \leq 80^\circ$, namely, $|r_{\rm tri}(\theta_0)|^2 < -23.9$ dB $\approx 0.41\%$, $|t_{\rm tri}(\theta_0)|^2 > -0.251$ dB $\approx 94.3\%$, and respectable concurrence between theoretical and full-wave results of transmission phase. Overall these excellent observations thoroughly validate our theory and design procedure and show that the perfect GHC can be accurately achieved in practice.

IV. Conclusion

To conclude, we have thoroughly formulated and validated the notable utility of the perfect GHC to devise planar omnidirectionally transparent radome functionalities. In particular, we have rigorously demonstrated how the scattering properties of thin trilyered admittance-sheet cascades at grazing angles determine universal ties between their physical constituents and their underlying effective microscopic susceptibilities applicable to the entire angular range. Importantly, our formalism reveals that effective normal responses, which are often overlooked in common Huygens' MS frameworks, inevitably arise in such configurations due to nonlocal mechanisms. These insightful closed-form expressions elucidate the existence and optimality of such solutions and simplify the design procedure.

Furthermore, we have harnessed these profound observations to craft a judicious and accurate method to design practical reflectionless PCB MS radomes that satisfy both the necessary parts of the GHC at once: vanishing reflection at grazing (balanced tangential polarizations) and normal (balanced tangential and normal polarizations) incidence scenarios. It is observed that such a scheme yields relatively convenient tunabilty by the available degrees of freedom and excellent performance. Overall, besides benefiting the domain of multilayered MS radomes at microwave frequencies, the universality of this work entails appreciable potential to inspire corollaries in other fields that require wide-angle transparency of structures to waves, for example, different radome configuration of other highly durable materials, other nonplanar shapes, and other types of waves (optical, acoustic, etc.).

References

[1] R. U. Nair and R. M. Jha, "Electromagnetic design and performance analysis of airborne radomes: Trends and perspectives [Antenna Applications Corner]," *IEEE Antennas Propag. Mag.*, vol. 56, no. 4, pp. 276–298, Aug. 2014.

[2] E. Öziş, A. V. Osipov, and T. F. Eibert, "Metamaterials for microwave radomes and the concept of a metaradome: Review of the literature", *Int. J. Antennas Propag.*, vol. 2017, p. 1356108, Jul. 2017.

[3] M. E. MacDonald, "An overview of radomes for large ground-based antennas," *IEEE Aerosp. Electron. Syst. Mag.*, vol. 34, no. 10, pp. 36–43, Oct. 2019.

[4] B.A. Munk, *Frequency Selective Surfaces: Theory and Design*, New York, NY: John Wiley and Sons, 2000.

[5] J. D. Ortiz, J. D. Baena, V. Losada, F. Medina, and J. L. Araque, "Spatial angular filtering by FSSs made of chains of interconnected SRRs and CSRRs," *IEEE Microw. Wirel. Compon. Lett.*, vol. 23, no. 9, pp. 477–479, Sept. 2013.

[6] A. Shaham and A. Epstein, "Systematic design of metasurface angular filters", *2022 IEEE Int. Symp. Antennas Propag. USNC-URSI Radio Sci. Meet. (AP-S/URSI)*, Denver, CO, Jul. 2022, pp. 569–570.

[7] D. F. Sievenpiper, "Nonlinear grounded metasurfaces for suppression of high-power pulsed RF currents," *IEEE Antennas Wirel. Propag. Lett.*, vol. 10, pp. 1516–1519, 2011.

[8] A. Benini, E. Martini, S. Monni, M. C. Viganò, F. Silvestri, E. Gandini, G. Gerini, G. Toso, and S. Maci, "Phase-gradient meta-dome for increasing grating-lobe-free scan range in phased arrays," *IEEE Trans. Antennas Propag.*, vol. 66, no. 8, pp. 3973–3982, Aug. 2018.

[9] A. Monti, S. Vellucci, M. Barbuto, D. Ramaccia, M. Longhi, C. Massagrande, A. Toscano, and F. Bilotti, "Quadratic-gradient metasurface-dome for wide-angle beam-steering phased array with reduced gain loss at broadside," *IEEE Trans. Antennas Propag.*, vol. 71, no. 2, pp. 2022–2027, Feb. 2023.

[10] T. R. Cameron and G. V. Eleftheriades, "Analysis and characterization of a wide-angle impedance matching metasurface for dipole phased arrays," *IEEE Trans. Antennas Propag.*, vol. 63, no. 9, pp. 3928–3938, Sept. 2015.

[11] R. Basiry, H. Abiri, and A. Yahaghi, "Electromagnetic performance analysis of omega-type metamaterial radomes," *Int. J. RF and Microw. Comput.-Aided Eng.*, vol. 21, no. 6, pp. 665–673, Sept. 2011.

[12] Y. He and G. V. Eleftheriades, "A thin double-mesh metamaterial radome for wide-angle and broadband applications at millimeter-wave frequencies," *IEEE Trans. Antennas Propag.*, vol. 68, no. 3, pp. 2176–2185, Mar. 2020.

[13] A. Shaham and A. Epstein, "Generalized Huygens' condition as the fulcrum of planar nonlocal omnidirectional transparency: from meta-atoms to metasurfaces," *arXiv preprint*, arXiv:2309.07294, Sept. 2023.

[14] A. Love, "Some highlights in reflector antenna development," *Radio Sci.*, vol. 11, pp. 671–684, 1976.

[15] P. Jin and R. W. Ziolkowski, "Metamaterial-inspired, electrically small Huygens sources", *IEEE Antennas Wirel. Propag. Lett.*, vol. 9, pp. 501–505, May 2010.

[16] C. Pfeiffer and A. Grbic, "Metamaterial Huygens' surfaces: Tailoring wave fronts with reflectionless sheets," *Phys. Rev. Lett.*, vol. 110, no. 19, p. 197401, May 2013.

[17] F. Monticone, N. M. Estakhri, and A. Alù, "Full control of nanoscale optical transmission with a composite metascreen," *Phys. Rev. Lett.*, vol. 110, no. 20, p. 203903, May 2013.

[18] M. Selvanayagam and G. V. Eleftheriades, "Discontinuous electromagnetic fields using orthogonal electric and magnetic currents for wavefront manipulation," *Opt. Express*, vol. 21, no. 12, p. 14409, Jun. 2013.

[19] A. Epstein and G. V. Eleftheriades, "Huygens metasurfaces via the equivalence principle: design and applications," *J. Opt. Soc. Am. B*, vol. 33, no. A31, Jan. 2016.

[20] M. Idemen, "Universal boundary relations of the electromagnetic field," *J. Phys. Soc. Jpn.*, vol. 59, no. 71, Jan. 1990.

[21] S. A. Tretyakov, *Analytical Modeling in Applied Electromagnetics*, Boston, MA: Artech House, 2003.

[22] E. F. Kuester, M. A. Mohamed, M. Piket-May, and C. L. Holloway, "Averaged transition conditions for electromagnetic fields at a metafilm," *IEEE Trans. Antennas Propag.*, vol. 51, no. 10, pp. 2641–2651, Oct. 2003.

[23] K. Achouri, M. A. Salem, and C. Caloz, "General metasurface synthesis based on susceptibility tensors," *IEEE Trans. Antennas Propag.*, vol. 63, no. 7, pp. 2977–2991, Apr. 2015.

[24] G. L. Matthaei, L. Young, and E. L. T. Jones, *Microwave Filters, Impedance-Matching Networks, and Coupling Structures* Dedham, MA: Artech House, 1980.

[25] S. Winder, *Analog and Digital Filter Design*, Amsterdam, Netherlands: Newnes, 2002.

[26] D. M. Pozar, *Microwave Engineering*, 4th ed., Hoboken, NJ: Wiley, 2012.

[27] A. Epstein and G. V. Eleftheriades, "Arbitrary power-conserving field transformations with passive lossless omega-type bianisotropic metasurfaces," *IEEE Trans. Antennas Propag.*, vol. 64, no. 9, pp. 3880–3895, Sept. 2016.

[28] C. Pfeiffer and A. Grbic, "Millimeter-wave transmitarrays for wavefront and polarization control," *IEEE Trans. Microw. Theory Techn.*, vol. 61, no. 12, pp. 4407–4417, Dec. 2013.

[29] C. Pfeiffer and A. Grbic, "Bianisotropic metasurfaces for optimal polarization control: analysis and synthesis," *Phys. Rev. Appl.*, vol. 2, no. 4, p. 044011, Oct. 2014.

[30] K. Shastri, F. Monticone, "Nonlocal flat optics," *Nat. Photon.*, vol. 17, pp. 36–47, 2023.

[31] D. Zaluški, A. Grbic, and S. Hrabar, "Analytical and experimental characterization of metasurfaces with normal polarizability," *Phys. Rev. B*, vol. 93, no. 155156, Apr. 2016.